# Measurements of Mean Velocity and Turbulent Intensities in a Free Isothermal Swirling Jet

J. P. Sislian* and R. A. Cusworth†
*University of Toronto, Toronto, Ontario, Canada*

**The objectives of the present measurements are to provide data against which results of numerical prediction procedures can be compared, and quantitative information on the behavior of all turbulent stresses and their correlation to spatial distribution of mean velocity gradients, with a view to improving our understanding of relevant transport processes and to guiding turbulence modeling and prediction efforts of such flows. A laser velocimeter, operating in a constant time interval sampling mode, was used to obtain the measurements. Measured values are presented for the case of strong swirling velocities (with recirculating region). The location and extent of the recirculation region is established. Contours of turbulent kinetic energy, derived from measured data, locate the high-turbulence intensity zones (i.e., zones of intense mixing). Experimental data indicate a strong dependence of the turbulent stresses on the local strain of the mean flow in most regions of the flow, which suggests that an eddy viscosity type of turbulence model, e.g., the $k$-$\epsilon$ model, rather than a Reynolds stress model could be acceptable for the prediction of such flows.**

## Nomenclature

$a,b,c$ = probe volume major and minor axes, respectively
$D$ = nozzle exit diameter
$d_1$ = laser beam waist diameter, = 1.1 mm
$f$ = focal length of transmitting optics lens, = 300 mm; frequency
$k$ = turbulent kinetic energy; nondimensional turbulent kinetic energy
$N$ = number of cycles counted by processor; number of data points measured in a sample
$\hat{n}$ = sensitivity vector
$r$ = radial distance
$S$ = swirl number
$\bar{u},\bar{v},\bar{w}$ = mean axial, radial, and circumferential velocity components, respectively
$x$ = longitudinal distance
$\alpha,\beta,\gamma$ = angles formed by sensitivity vector with coordinate axes
$\delta_f$ = fringe spacing, = 2.75 $\mu$m
$\lambda$ = laser radiation wavelength, = 632.8 nm
$\theta$ = total angle formed by intersecting laser beams; = 13.3 deg
$\nu_D$ = Doppler frequency
$\rho$ = fluid density
$\psi$ = stream function
$\psi_0$ = exit mean mass flow rate

*Superscripts*

$(\bar{\ })$ = time-averaged value
$(\ )'$ = fluctuating quantity

## Introduction

MOST combustion systems of practical interest, such as gas turbine engine combustors, boilers, and furnaces, involve large regions of recirculating flows. Recirculation zones provide the heat source, by upstream convection and mixing of hot reaction products with an oncoming fuel and airstream, and the reduced velocity necessary for flame stabilization. Such zones are formed when an adverse axial pressure gradient exceeds the momentum of the fluid flow. This can be brought about by several means, e.g., by imparting a rotational motion to the fluid. Such swirling flows form a fundamental part of the gasdynamics of many combustors. It is known that swirl has marked effects on the flowfield, affecting the rate of spread of the jet, the length, shape, and stability of the flame, and the combustion intensity. The mixing region between the fuel jet and the ambient fluid is characterized by considerable turbulence production, and its turbulence structure is greatly affected by the amount of swirl introduced.

A realistic simulation and solution of swirling, recirculating, turbulent combusting flows in combustors is a difficult task. While a number of attempts have recently been made to model such flows mathematically,[1,2] the efforts so far carried out have been relatively crude, chiefly as a result of the models of the turbulence and the chemical reaction processes used. There is little doubt that the greatest impediment to developing a viable mathematical model of such flows is the inadequacy of the physical models. In almost all combustion situations considered so far, turbulence models employed assumed extended forms of isothermal cases, which in turn are represented by some form of eddy viscosity formulation. The most typically used is the so-called $k$-$\epsilon$ two-equation model of turbulence, the flame/turbulence interaction being represented by simple expressions lacking rigorous formulation.[1,2] While these models provide predictions of adequate accuracy for certain relatively simple isothermal and combusting turbulent flow situations, experiments[3,4] and calculations of exchange coefficients from mean value distributions[5,6] have shown that, for swirling flows, the turbulent stress distributions are anisotropic.

A considerable aid to modeling efforts is the creation of an extensive and detailed data base for such quantities as the mean and fluctuating levels of velocity, temperature, density, concentrations, and their correlations in strongly swirling

Received June 6, 1984; revision received June 14, 1985. 

*Research Associate, Institute for Aerospace Studies. Member AIAA.
†Graduate Student, Institute for Aerospace Studies.

turbulent combusting flows. Such data are practically nonexistent. Even data on mean and fluctuating levels of velocity and their correlations, i.e., Reynolds stresses, are scarce and insufficient to allow a satisfactory turbulence modeling of momentum equations. Syred et al.[3] used hot-wire anemometers to measure mean velocity and all turbulent stress tensor components in a very strongly swirling free isothermal jet and from these values derived effective viscosity distributions. These distributions showed significant radial variations and considerable anisotropy of turbulence. By hot-wire anemometry, Ribeiro and Whitelaw[7] measured magnitudes of mean velocity components, all turbulent stress tensor components and probability density distributions of fluctuating velocity for isothermal turbulent coaxial jets, with and without swirl, emerging into stagnant surroundings. Vu and Gouldin[8] report measurements in a model combustor composed of two confined coaxial swirling jets under noncombusting conditions. Directional pitot probe and hot-wire anemometry were used to determine mean axial and swirl velocities and the fluctuating velocity component parallel to the mean velocity for co- and counterswirl conditions. Many problems encountered by the use of probes and hot-wire anemometry in complex turbulent isothermal and combusting flowfield measurements were overcome by the advent of the linear, nonintrusive technique of laser-Doppler velocimetry (LDV). Attempts at using LDV as applied to turbulent, swirling, isothermal and combusting flows have already been reported in the literature.[9-13] Baker et al.[9] measured values of three components of mean velocity and the corresponding normal turbulent stresses in a confined, axisymmetric, swirling flow configuration in a cylindrical enclosure for both isothermal and combusting cases. Their results indicate the nonisotropy of turbulence in the isothermal flows, the increase of the nonisotropy regions in the combusting flow, and the need for consideration of the three normal turbulent stresses in appropriate turbulence models. In Ref. 10 an unconfined turbulent swirling jet under flame and no-flame conditions is considered. Axial and circumferential components of the mean velocity were measured, as well as the three normal turbulent stresses. It was found that the kinetic energy of turbulence per unit mass in the combusting flow was higher than in the corresponding cold flow in almost all regions of the flame. Reference 11 represents the first attempt at using the LDV technique in measuring the three mean velocity and all the six turbulent stress tensor components in an unconfined swirling jet under isothermal and combusting conditions. The results indicate that turbulence levels are increased as a consequence of combustion; that regions of anisotropy of turbulence are significant, particularly in the reacting flow; and that the local equilibrium turbulence model may be used in predicting strongly swirling jet flow with and without combustion. Unfortunately, the data presented contain significant scatter both in isothermal and combusting flow situations, and it is virtually impossible to infer even the general behavior of certain turbulent stress components. Gouldin et al.[12] and Sommer[13] have investigated nearly similar flow configurations of two confined, concentric co- and counterswirling jets in a cylindrical combustor with and without combustion. Measurements were reported of axial and circumferential mean velocity components and of the corresponding turbulent normal stresses in co- and counterswirl situations. Sommer used a two-component (two-color) laser Doppler velocimeter to simultaneously measure axial and circumferential velocity components and was thus able to present, in addition, data on one turbulent shear stress component.

The present paper is concerned with laser Doppler velocimetry measurements of the three mean velocity and the six turbulent stress tensor components in a free isothermal swirling jet. The main emphasis is on providing quantitative information on the behavior and evolution of all turbulent stresses in the flowfield and their correlation to spatial distribution of gradients of mean velocity components. Another objective is to provide data against which results of numerical prediction procedures can be compared.

## Experimental Apparatus and Instrumentation

A 685 mm long, 76.2 mm i.d. circular duct containing fine mesh screens connects the settling chamber with the contoured jet nozzle of 25.4 mm exit diameter. Swirling motion is imparted to the axial flow by fixed, flat guide vane swirlers placed at the nozzle exit. The constancy of the flow rate at the exit of the jet was checked by measuring the exit centerline axial velocity in the nonswirling jet flow at regular time intervals during a period of approximately 2 h. Exit centerline axial velocities were also measured before and after each experimental session. In all cases, the discrepancy between such measured values was always well within the accuracy limits of the measuring technique. The axial symmetry of the flow was assessed by measuring exit axial and circumferential mean velocity components up to a distance of ⅓ in. on both sides of the geometrical axis of symmetry. Their relative error, at the corresponding symmetric positions, was of the order of 6%. The swirl number $S$, which characterizes the intensity of the swirl,[14] was calculated from measured exit axial and circumferential mean velocity components. The swirling jet flow facility was placed vertically on the lower rigid frame of a three-dimensional traversing mechanism. The traversing mechanism displaced the optical table in two mutually perpendicular horizontal directions and in the vertical direction. The positioning accuracy of the traversing mechanism was $\pm 0.125$ mm in the horizontal directions and approximately $\pm 1$ mm in the vertical direction. The range of travel was 200 mm in the horizontal and 500 mm in the vertical directions.

The swirling jet flow was seeded with maize oil particles by diverting part of the supply airstream, through a pressure regulator and a filter, to the TSI Model 3076 constant output atomizer. From the atomizer, oil droplets were led into the settling chamber diametrically to mix with the main air. For the range of atomizer pressure settings used, the mean oil droplet diameter (previously determined from a special laser Doppler velocimeter set up by the so-called visibility method) ranged from 0.8 to 1.0 $\mu$m. This particle diameter range is appropriate in gas flows in which turbulence frequencies exceeding 1 kHz are to be followed.[15] The entrained atmospheric airflow was not seeded.

The optical arrangement of the laser Doppler velocimetry system with a Bragg cell has been built up from standard DISA 55X Modular Optics components. A 15 mW Spectra Physics Model 124B helium-neon laser (wavelength $\lambda = 632.8$ nm; beam diameter $d_1 = 1.1$ mm) provided the monochromatic and coherent light source. The two beams of equal intensity emerging from the transmitting optics through an $f = 300$ mm focal length lens intersect at an angle $\theta = 13.3$ deg. The spacing of the interference fringes in the probe volume is $\delta_f = 2.73 \times 10^{-6}$ m. The ellipsoidal probe volume dimensions are: $a = 9.785 \times 10^{-4}$ m, $b = 1.142 \times 10^{-4}$ m, and $c = 1.134 \times 10^{-4}$ m. The number of fringes in the probe volume is $N_f = 42$. The entire laser Doppler system was carefully aligned and rigidly mounted to the optical table of the traversing gear, which made it quite stable. The transmitting optics can be rotated 360 deg; the maximum lateral displacement of the probe volume from the axis of rotation, when the system was rotated, was less than 0.1 mm.

The photomultiplier output signal carrying the sum of the Doppler frequency $\nu_D$ and the constant optical frequency $\nu_0 = 40$ MHz was fed to the DISA 55N10 Electronic Frequency Shifter, to shift the signal frequency up or down to a desired level. The electronic mixer output signals were analyzed by a TSI Counter Processor, Model 1980A. The photomultiplier signal and/or the filtered-out signal (from the processor) was continuously monitored on a Hewlett

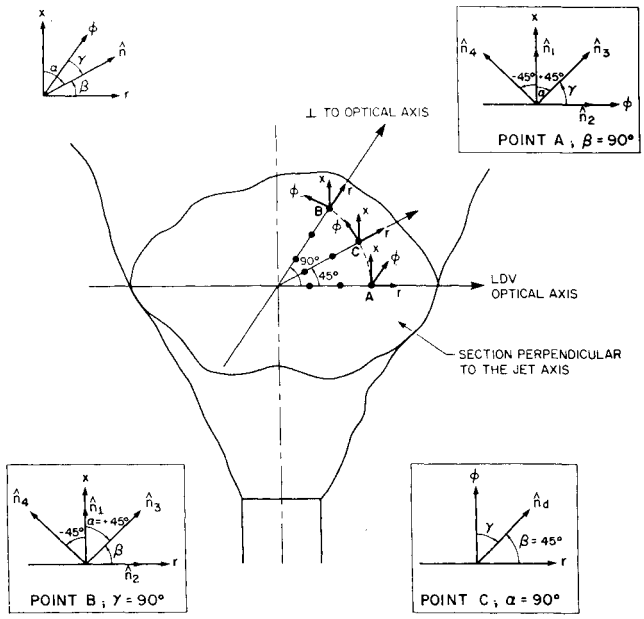


**Fig. 1 Flow system geometry for evaluation of laser-Doppler measurements.**

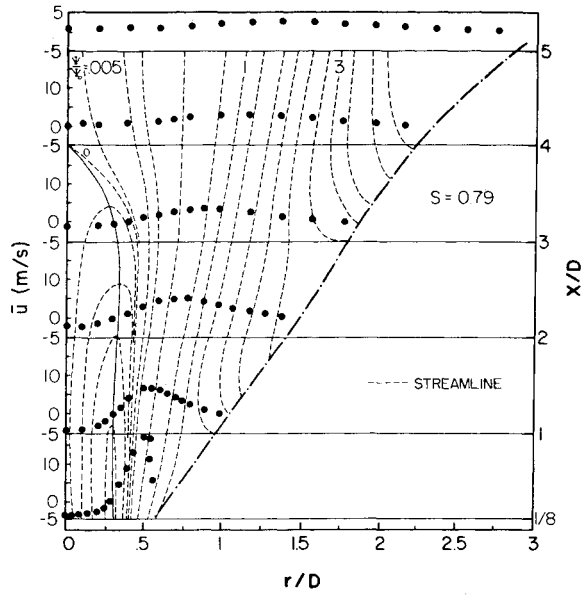


**Fig. 2 Distributions of mean axial velocity component.**

Packard 1744A oscilloscope. A microcomputer system was developed to read and process the data from the TSI 1980A counter. The reduced data were displayed on the CRT terminal and then dumped onto an on-line printer. The data reduction process is quite fast and efficient and permits on-line CRT graphics display with hard-copy capabilities.

Figure 1 shows the flow system geometry adopted in the present investigation to evaluate the local mean flow velocity components and the various correlations of the fluctuating velocity components. The magnitude of the instantaneous Doppler frequency

$$\nu_D = \frac{V}{\lambda} \cdot (\hat{e}_1 - \hat{e}_2) = \frac{V}{\lambda} \cdot \hat{n} 2\sin\frac{\theta}{2}$$

where $\hat{e}_1$ and $\hat{e}_2$ are the unit vectors in the direction of the two intersecting laser beams, and $\hat{n}$, the unit "sensitivity"

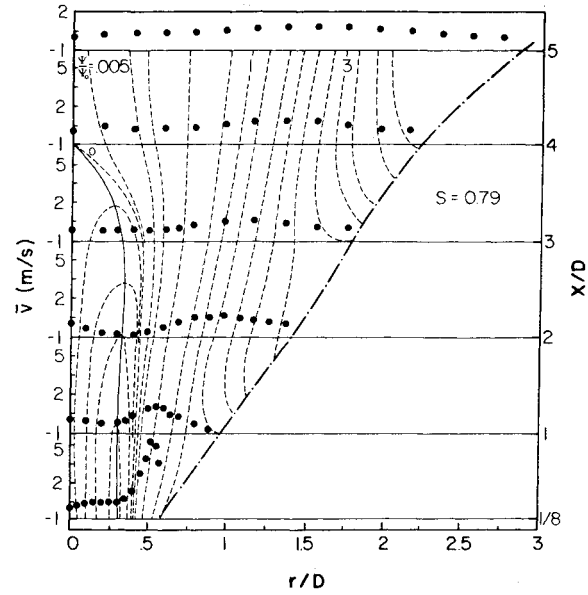


**Fig. 3 Distributions of mean radial velocity component.**

vector perpendicular to the plane fringes, was evaluated in a coordinate system $x,r,\phi$, with the origin at the center of the probe volume, the $x$ axis parallel to the (vertical) axis of symmetry of the flow, the $r$ axis in the radial direction, and the $\phi$ axis perpendicular to both of them. In any horizontal section considered, the probe volume was moved, starting from the axis of symmetry, in the direction of the optical axis of the LDV system. At each measurement point A in the flowfield along this direction, the unit vector $\hat{n}$ was placed vertically ($\alpha=0$ deg, $\beta=\gamma=90$ deg; $\alpha,\beta,\gamma$ are the angles formed by the sensitivity vector with the coordinate axes, as in Fig. 1) and the mean axial velocity component $\bar{u}$ and the turbulent stress $\overline{u'^2}$ were determined. The LDV optical system was then rotated until $\hat{n}$ was in the plane $(r,\phi)$, ($\alpha=\beta=90$ deg and $\gamma=0$ deg). The mean velocity component $\bar{w}$ and the corresponding turbulent normal stress $\overline{w'^2}$ were computed. Next, the optical system was rotated $+45$ deg and then $-45$ deg. The turbulent shear stress $\overline{u'w'}$ was then calculated from the equation

$$\overline{u'w'} = (\overline{V_+'^2} - \overline{V_-'^2})/2$$

where $\overline{V_+'^2}$ and $\overline{V_-'^2}$ are the mean squares of the total velocity fluctuations in $+45$ and $-45$ deg directions, respectively.

After traversing the flowfield in this direction, the probe volume was brought back to the axis of symmetry of the flow and moved in a direction perpendicular to the optical axis of the LDV. At each measurement point B in this direction (see Fig. 1), the sensitivity vector was given the vertical position, the position in the horizontal plane $(r,\phi)$, and then the position $\pm 45$ deg around the $x$ axis. The quantities $\bar{v}$, $\overline{v'^2}$, and $\overline{u'v'}$ were computed in a manner similar to that used in traversing the flow in the optical axis direction.

In order to determine the remaining turbulent shear stress $\overline{v'w'}$, the flow was traversed a third time along the bisector of the right angle formed by the last two directions. The vector $\hat{n}$ was placed in the horizontal $r,\phi$ plane [$\alpha=90$ deg, $\beta=45$ deg, $\gamma=(\pi/2)-45$ deg] for all measurement points C (see Fig. 1), and the probe volume positioned consecutively at the same distances from the axis of symmetry as the corresponding measurement points on the previous two directions. At each point C along this direction we have

$$\overline{V_C'^2} = [(\overline{v'^2} + \overline{w'^2})/2] + \overline{v'w'}$$

where $\overline{V_C'^2}$ is the mean square of total velocity fluctuations.

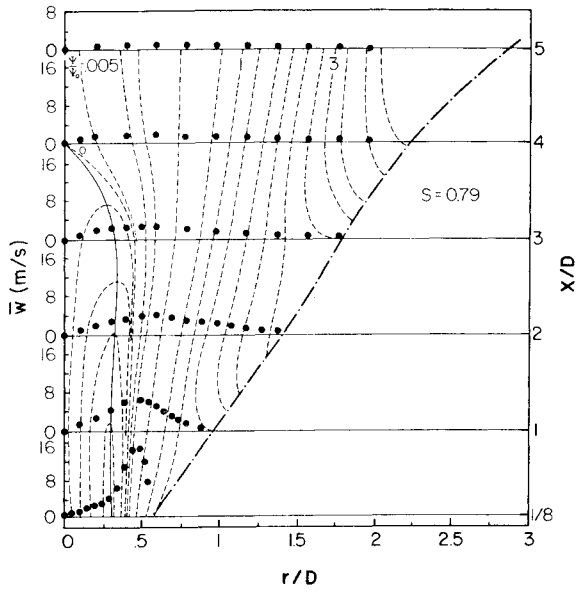


**Fig. 4 Distributions of mean circumferential velocity component.**

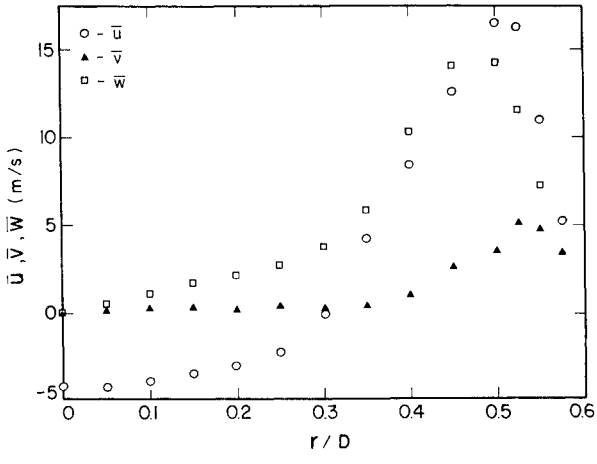


**Fig. 5 Radial distributions of mean velocity components: $X/D = 0.125$, swirling jet, $S = 0.79$.**

If we assume that the values of $\overline{v'^2}$ and $\overline{w'^2}$ at point C in the axisymmetric flow are equal to those measured at points A and B, then we can deterime $\overline{v'w'}$ from the equation

$$\overline{v'w'} = \overline{V_C'^2} - [(\overline{v_B'^2} + \overline{v_A'^2})/2]$$

Thus, all the mean velocity and turbulent stress tensor components were determined at the measurement points in the considered section of the flowfield. For each data point, 2000 individual realizations were averaged. All data greater than $\pm 3\sigma$ from its mean were rejected. Here, $\sigma$ is the standard deviation.

The effective number of fringes in the probe volume depends on the amount of electronic frequency shift used and the flow velocity at the measurement point. In order to minimize errors in frequency measurements due to noise, the maximum possible number of signal cycles $N$, compatible with the desired data rate, were used. In general, in relatively high-velocity regions in the flow, the number of signal cycles timed for frequency measurements was set to $N = 16$, whereas in low-velocity regions of the flow, $N$ was set to 32, the maximum number of measurable cycles for the TSI Model 1980A processor. Values of $N$ lower than the above number of signal cycles, as well as the so-called total burst mode (all cycles of the Doppler signal used to measure the instantaneous frequency) were not used in the present experiments. The average data rates (as monitored by the TSI 1980 processor) were 5000/s in the central portion of the flow and about 100/s at the edges of the flow.

It is well known that statistical parameters obtained from instantaneous frequency measurements by counting techniques of individual Doppler signals are subject to biases from several sources (see, e.g., Ref. 15), the most significant of these being the so-called velocity bias. Several correction schemes have been proposed (see Refs. 16-19). Unfortunately, there is still considerable disagreement as to the proper correction approach. In the present work, the error caused by velocity bias was minimized by following the approach used in Ref 20. An ensemble average will approximate a time average if the sampling of the velocity history is performed at equal or nearly equal time intervals. It is possible to obtain a close approximation to sampling at equal time increments by controlling the relationship between the data rate, as displayed by the TSI processor, and the computer speed, i.e., the number of data per second that the microcomputer processes. In the data acquisition system used in the present investigation, the data acquisition rate by the computer was made variable, so as to always keep an approximate ratio of 10:1 between the processor data rate and the computer data acquisition rate (i.e., the computer sampled 1 out of 10 validated data points supplied by the processor). When the computer is ready for data, the processor will have it ready in a very short time due to the high processor data rate. As a result, the actual sampling is performed at nearly equal time intervals. In Ref. 20, it is shown that measurements performed in this way coincide with randomly sampled measurements corrected according to McLaughlin and Tiederman's one-dimensional velocity weighing.[16] No other attempts have been made, in the present experiments, to correct for velocity bias or for any other biases, such as the nonuniform seeding bias, the incomplete signal bias, and the velocity gradient bias.[21] The last two biasing errors in the present data are considered to be small because of the significant amount of frequency shift used and the relative smallness of the probe volume, respectively.

It is difficult to assess the accuracy of laser velocimeter measurements in turbulent flows due to sources of potential signal biasing (at least 10 such sources are cited in Ref. 21). However, by paying careful attention to the choice of components of a laser velocimeter and to their integration, most of the biases can virtually be eliminated. Based on a rough estimate of various significant sources of error in the present optical and signal processing arrangement, it is suggested that expected uncertainties in mean velocity measurements are of the order of 3-4% (slightly higher for the $\bar{v}$ component), in normal Reynolds stresses of the order of 5%, in the $xr$ and $x\phi$ components of the Reynolds shear stress of the order of 8%, and in the $r\phi$ component of $\sim 10\%$.

## Measurements and Discussion

Measured values are presented for the case of a strongly swirling jet, $S = 0.79$. The exit Reynolds number, based on the average axial velocity at the exit, $\bar{u}_0 = 4Q_0/\pi D^2$, where $Q_0$ is the exit volumetric flow rate and $D$ the nozzle exit diameter, was $1.16 \times 10^4$ for an average velocity of 6.8 m/s. Measurements were performed at distances $x/D = 0.125$, 1.0, 2.0, 3.0, 4.0, and 5.0 downstream of the nozzle exit. The mean streamlines of the flow, calculated by integrating mean axial velocity components

$$\psi = 2\pi \int_0^r \rho \bar{u} dr, \quad \psi_0 = 2\pi \int_0^R \rho \bar{u} dr$$

are plotted as dashed lines on all figures.

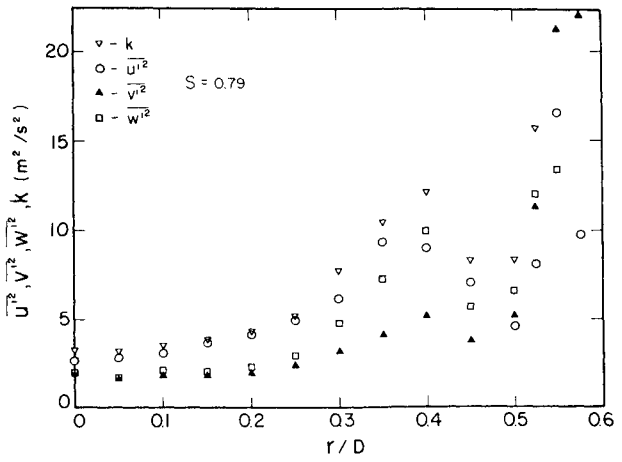


**Fig. 6 Radial distributions of normal Reynolds stresses and turbulent kinetic energy: $X/D = 0.125$.**

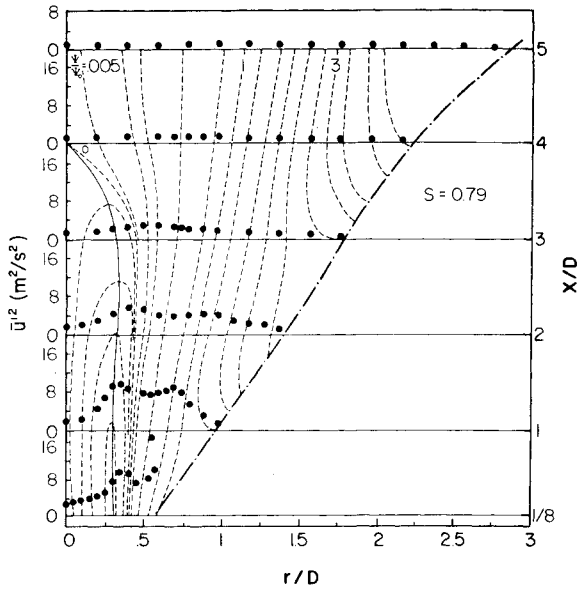


**Fig. 7 Distributions of axial Reynolds stress.**

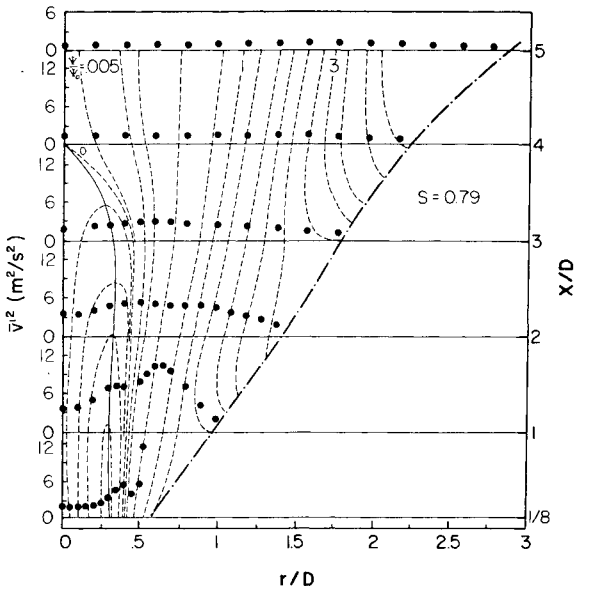


**Fig. 8 Distributions of radial Reynolds stress.**

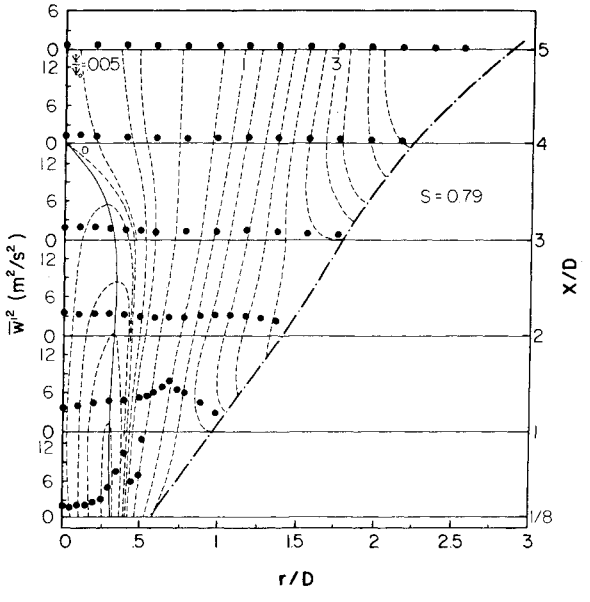


**Fig. 9 Distributions of circumferential Reynolds stress.**

Figures 2-4 represent radial distributions of mean velocity components. The maximum values of the positive mean axial velocity components move outward and decay as we proceed downstream in the flow. At $x/D = 5.0$ (Fig. 2), the mean axial velocity distribution has already the well-known hump-type shape peculiar to the far downstream regions of strongly swirling jets. The radial component of the mean velocity is small (Fig. 3); it is negative in the recirculation bubble and positive outside it. As is the case with the mean axial velocity component, its maximum at the edge of the jet, at the exit, moves radially outward and decays at subsequent downstream sections. The exit profile of the mean circumferential velocity component $\bar{w}$ (Fig. 4) consists of two parts: the inner part, within the recirculation zone, has a linear, rigid body rotation distribution; in the outer main swirling flow region, $\bar{w}$ reaches maximum at the edge of the flow and then decreases rapidly. Inside the recirculation zone, the fluid rotates as a rigid body; the angular velocity of this rigid body rotation increases initially, reaching a maximum at $x/D = 1.0$, and then decreases gradually with downstream distance. At approximately $x/D = 1.0$, a transition takes place from the exit profile to the Rankine vortex profile. Maximum swirl velocities occur outside the recirculation region. The radial positions of these maxima move radially outward and decay rapidly. The positions of maxima of radial gradients of mean axial and circumferential velocity components approximately coincide with the zero velocity line in the recirculation zone, up to a distance $x/D \cong 2.0$. Radial distributions of mean velocity components at the exit, $x/D = 0.125$, are shown in Fig. 5.

Double peak values of normal Reynolds stresses and, hence, of turbulent kinetic energy were found at the exit section (Fig. 6). Similar double peak values have also been reported in Ref. 11. These peaks are produced in regions with high gradients of mean velocity. Measurements show that the inner peak values of normal Reynolds stresses are located close to the zero streamline (i.e., near the edge of the recirculation zone). The outer peak (maximum) values are due to the shear layer at the edge of the jet flow. These double peak values of $\overline{u'^2}$ persist up to a distance $x/D = 2$-3, the outer peak value decaying more rapidly than the inner (Fig. 7). The double peak values of $\overline{v'^2}$ also persist up to the same distance, but although the outer peak decays, the inner peak value first increases (Fig. 8) and then decays slowly at subsequent downstream sections. Inner peak values of

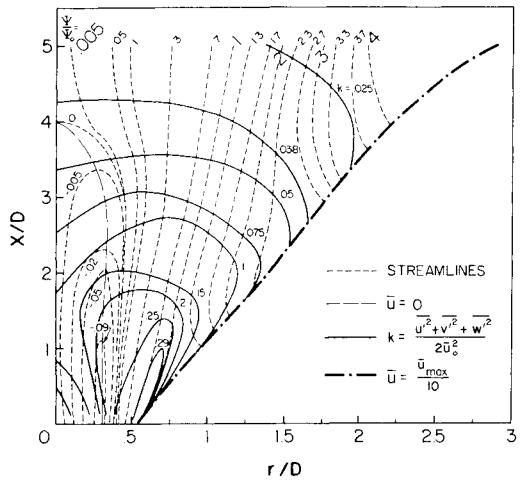


Fig. 10 Contours of turbulent kinetic energy.

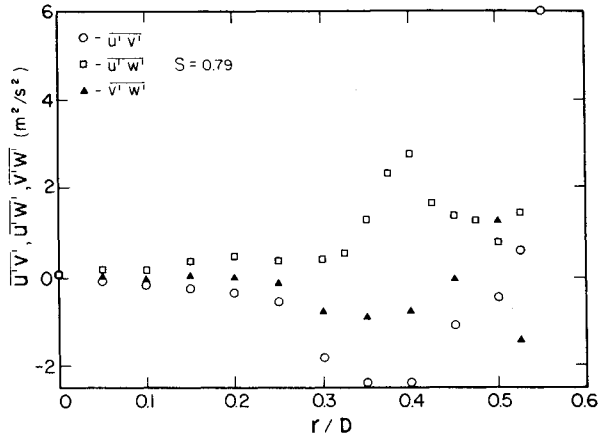


Fig. 11 Radial distributions of Reynolds shear stresses: $X/D = 0.125$.

$\overline{u'^2}$ and $\overline{v'^2}$ remain near the edge or move slightly inside the recirculation zone up to $x/D \cong 2.0$. Downstream, they clearly fall outside the recirculation zone.

The inner peak value of $\overline{w'^2}$ (Fig. 9) decays very rapidly and has almost disappeared at $x/D = 1.0$. Further downstream, the distributions of normal stresses gradually approach those in a weakly swirling jet. Their magnitudes are quite small at distances $x/D = 4$-5. The distributions of kinetic energy of turbulence are similar to those of normal stresses. Contours of nondimensional turbulent kinetic energy are depicted in Fig. 10. The figure shows that the maximum turbulence is generated in the shear layer existing at the edge of the swirling jet flow immediately after the exit. High values of turbulent kinetic energy also exist near the zero streamline at the exit. The kinetic energy of turbulence decays rapidly in the axial and radial directions as the swirling jet expands rapidly into the stagnant surroundings. Except at the exit section, the $\overline{u'^2}$ and $\overline{v'^2}$ stresses are, in general, larger than $\overline{w'^2}$; up to a distance $x/D \cong 2.0$, $\overline{v'^2}$ is larger than $\overline{u'^2}$ in the outer part of the flow and smaller in the inner region of the flow. Further downstream, $\overline{u'^2}$ and $\overline{v'^2}$ attain the same order of magnitude in the central region of the flowfield, with $\overline{v'^2}$ remaining larger than $\overline{u'^2}$ in the outer region. The magnitudes of the mean axial velocity and the axial turbulent stress obtained at all corresponding measuring stations A and B (see Fig. 1) were found to coincide within the accuracy limits of the measuring technique.

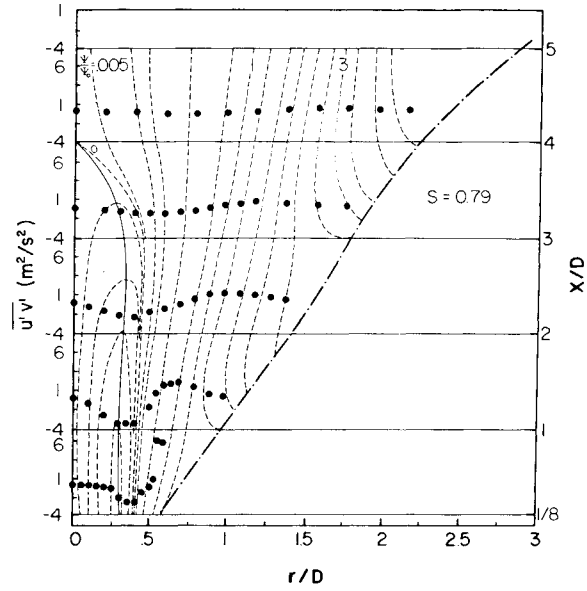


Fig. 12 Distributions of the $xr$-shear-stress component.

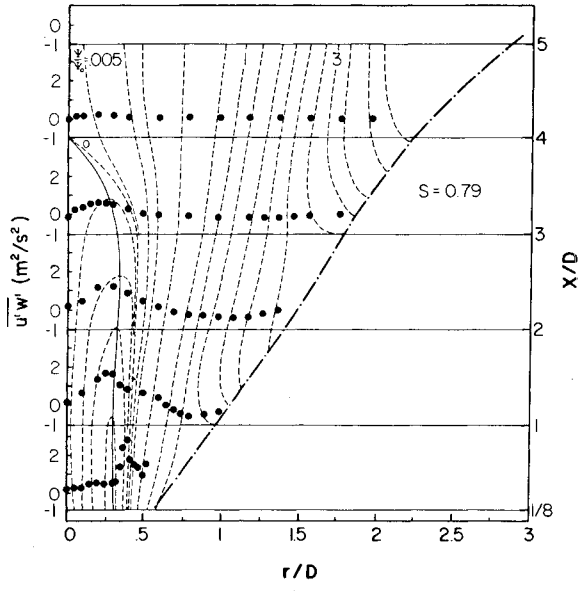


Fig. 13 Distributions of the $x\phi$-shear-stress component.

Reynolds shear stresses, presented in Figs. 11-14 are appreciably smaller than the normal stresses. At the exit section, Fig. 11, the distributions of shear stresses exhibit double peaks. The radial positions of the inner peak values, positive for the $\overline{u'w'}$ stresses and negative for $\overline{u'v'}$ and $\overline{v'w'}$ stresses, coincide with those of normal stresses, i.e., they are near the edge of the recirculation zone; the outer positive peaks are located in the jet flow boundary (shear) layer. Further downstream the shear stresses decay rapidly and become quite small at distances $x/D = 3.0$-4.0. Both peak values of $\overline{u'v'}$ decay at approximately the same rate. Their radial locations coincide with those of normal stress $\overline{u'^2}$ at all downstream sections (see Fig. 7); i.e., up to $x/D = 2.0$, the negative maxima of $\overline{u'v'}$ are near the edge of the recirculation zone and gradually move outward downstream. The shear stress $\overline{v'w'}$ is very small in the recirculation zone and attains its maximum value outside it. These maxima move gradually outward at downstream sections. Analysis of the measured data shows that at all sections where measurements were performed, radial positions where $\overline{u'v'}$ and $\partial\bar{u}/\partial r$ ap-

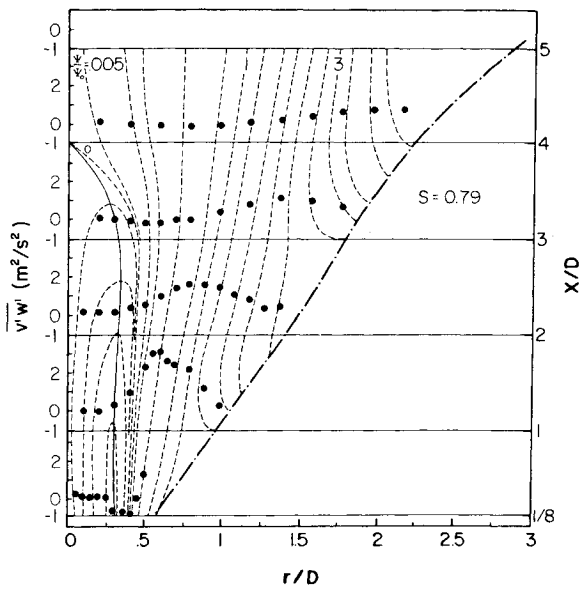


**Fig. 14 Distributions of the $r\phi$-shear-stress component.**

proach zero coincide. A similar conclusion has also been reached in Ref. 11. Moreover, radial positions of minima and maxima of these quantities also coincide at all sections. The same is true for the shear stress $\overline{v'w'}$ and $r\partial(\bar{w}/r)/\partial r$ up to the section $x/D=2.0$. Further downstream the above-noted coincidence of these latter quantities deteriorates. This remarkable experimental fact shows a strong dependence of these shear stresses on the local strain of the mean flow, and suggests an eddy viscosity type of turbulence model for these stresses rather than Reynolds stress modeling. Maxima of the shear stress $\overline{u'w'}$ are located in the recirculaton zone (see Fig. 13). The peak value of this stress at the initial section is located at the edge of the recirculation region. At subsequent sections, contrary to the behavior of the other stresses, these maxima move inward and decay rapidly. At distances $x/D\cong 3.0$-$4.0$, the magnitude of $\overline{u'w'}$ becomes very small. Radial locations of negative maxima of this stress seem to coincide with those of positive $\overline{u'v'}$ stress maxima.

Detailed measurements of the three components of the mean velocity and the six components of the turbulent stress tensor for the case considered, $S=0.79$, as well as for the cases of weakly swirling, $S=0.4$, and nonswirling, $S=0$, freejet flows, are given in Ref. 22.

## Conclusions

Measurements performed at $x/D=0.125$, 1, 2, 3, 4, and 5 provide a broad data base against which results of calculation procedures embodying various turbulence models can be compared. The normal Reynolds stress results show substantial deviations from isotropy; these stresses are significantly larger than the Reynolds shear stresses. This clearly indicates the need to consider the three normal stresses in any turbulence model of such flows. Maxima of these stresses occur in regions of high gradients of mean velocity, i.e., near the edge of the recirculation zone and in the boundary (shear) layer of the jet. Radial positions where the shear stress $\overline{u'v'}$ and $\partial\bar{u}/\partial r$ approach zero, maximum and minimum values coincide. The same is true for the stress $\overline{v'w'}$ and $r(\partial\bar{w}/r)/\partial r$ up to the middle portion of the investigated flow. These relationships indicate a strong dependence of these stresses on the local strain of the mean flow. Hence, an eddy viscosity type of turbulence model rather than a Reynolds stress model could be acceptable to predict such flows.

## Acknowledgments

This research was financially supported by the Natural Sciences and Engineering Research Council of Canada under Strategic Grant G0691, by Pratt and Whitney of Canada Ltd., Mississauga, Ontario, and by Energy, Mines and Resources, Canada. Their support is gratefully acknowledged.

## References

[1]Lilley, D. G., "Swirl Flows in Combustion: A Review," *AIAA Journal*, Vol. 15, Aug. 1977, pp. 1063-1078.

[2]Novick, A. S., Miles, G. A., and Lilley, D. G., "Numerical Simulation of Combustor Flowfields: A Primitive Variable Design Capability," *Journal of Energy*, Vol. 3, March-April 1979, pp. 95-105.

[3]Syred, N., Béer, J. M., and Chigier, N. A., "Turbulence Measurements in Swirling Recirculating Flows," Institute of Mechanical Engineering, London, Symposium on Internal Flow, Univ. of Salford, England, 1971, pp. B27-B36.

[4]Syred, N., Chigier, N. A., and Béer, J. M., "Flame Stabilization in Recirculating Zones of Jets with Swirl," *13th Symposium (International) on Combustion*, The Combustion Institute, Pittsburgh, PA, 1971, pp. 617-624.

[5]Lilley, D. G. and Chigier, N. A., "Nonisotropic Turbulent Stress Distribution in Swirling Flows from Mean Value Distributions," *International Journal of Heat & Mass Transfer*, Vol. 14, 1971, pp. 573-585.

[6]Lilley, D. G. and Chigier, N. A., "Nonisotropic Exchange Coefficients in Turbulent Swirling Flames from Mean Value Distributions," *Combustion and Flame*, Vol. 16, 1971, pp. 177-189.

[7]Ribeiro, M. M. and Whitelaw, J. H., "Coaxial Jets With and Without Swirl," *Journal of Fluid Mechanics*, Vol. 96, Pt. 4, 1980, pp. 769-795.

[8]Vu, B. T. and Gouldin, F. C., "Flow Measurements in a Model Swirl Combustor," AIAA Paper 80-0076, 1980; also, *AIAA Journal*, Vol. 20, May 1981, pp. 642-651.

[9]Baker, R. J., Hutchinson, P., Khalil, E. E., and Whitelaw, J. H., "Measurements of Three Velocity Components in a Model Furnace With and Without Combustion," *15th Symposium (International) on Combustion*, The Combustion Institute, Pittsburgh, PA, 1975, pp. 553-559.

[10]Chigier, N. A. and Dvorak, K., "Laser Anemometer Measurements in Flames with Swirl," *15th Symposium (International) on Combustion*, The Combustion Institute, Pittsburgh, PA, 1975, pp. 573-585.

[11]Fujii, S., Eguchi, K., and Gomi, M., "Swirling Jets With and Without Combustion," *AIAA Journal*, Vol. 19, Nov. 1981, pp. 1438-1442.

[12]Gouldin, F. C., Depsky, J. S., and Lee, S. L., "Velocity Field Characteristics of a Swirling Flow Combustor," AIAA Paper 83-0314, Jan. 1983.

[13]Sommer, H. T., "Swirling Flow in Research Combustor," AIAA Paper 83-0313, Jan. 1983.

[14]Béer, J. M. and Chigier, N. A., *Combustion Aerodynamics*, Applied Science Publishers Ltd., London, 1972, Chap. 5.

[15]Durst, F., Melling, A., and Whitelaw, J. H., *Principles and Practice of Laser-Doppler Anemometry*, Academic Press, New York, 1976, Chap. 9.

[16]McLaughlin, D. K. and Tiederman, W. G., "Biasing Correction for Individual Realization Laser Anemometer Measurements in Turbulent Flows," *Physics of Fluids*, Vol. 16, Dec. 1973, pp. 2082-2088.

[17]Durao, D. and Whitelaw, J. H., "The Influence of Sampling Procedures on Velocity Bias in Turbulent Flows," *Proceedings of the LDA Symposium*, Copenhagen, 1975, pp. 138-149.

[18]George, W. K. Jr., "Limitations to Measuring Accuracy Inherent in Laser Doppler Signal," *Proceedings of the LDA Symposium*, Copenhagen, 1975, pp. 20-63.

[19]Buchhave, P. and George, W. K. Jr., "Bias Corrections in Turbulence Measurements by the Laser Doppler Anemometer," Laser Velocimetry and Particle Sizing, *Proceedings of the 3rd International Workshop on Laser Velocimetry*, edited by H. D. Thompson and W. H. Stevenson, Hemisphere Publishing Corp., Washington, DC., 1979, pp. 110-119.

[20]Stevenson, W. H., Thompson, H. D., and Roesler, T., "Direct Measurement of Laser Velocimeter Bias Errors in a Turbulent Flow," *AIAA Journal*, Vol. 20, Dec. 1982, pp. 1720-1723.

[21]Thompson, H. D. and Flack, R. Jr., "An Application of Laser Velocimetry to the Interpretation of Turbulent Structure," *Proceedings of the ISL/AGARD Workshop on Laser Anemometry*, edited by H. J. Pfeiffer and J. Haertig, German/French Research Institute, St. Louis, France, 1976, pp. 189-231.

[22]Sislian, J. P. and Cusworth, R. A., "Laser Doppler Velocimetry Measurements of Mean Velocity and Turbulent Stress Tensor Components in a Free Isothermal Swirling Jet," UTIAS Rept. 281, 1984.